NANO LETTERS

2007
Vol. 7, No. 3
713−718

Effect of Spatial Confinement on the Glass-Transition Temperature of Patterned Polymer Nanostructures

Manish K. Mundra,[†] Suresh K. Donthu,[†] Vinayak P. Dravid,*[,†] and John M. Torkelson*[,†,‡]

Department of Materials Science and Engineering and Department of Chemical and Biological Engineering, Northwestern University, Evanston, Illinois 60208

Received December 10, 2006; Revised Manuscript Received January 28, 2007

ABSTRACT

Poly(methyl methacrylate) (PMMA) nanostructures embedded with a fluorescence tag are fabricated using electron beam lithography on oxidized silicon substrates. The glass transition temperatures (T_gs) of these one-dimensional (1-D) nanostructures (parallel lines) are measured by monitoring their temperature-dependent fluorescence intensities, revealing substantial differences between the T_gs of the nanostructures and the thin films from which they were fabricated. For example, the T_g of 50-nm-wide PMMA nanolines on silica is ~15 K lower than that of a PMMA film on silica of the same 18 nm thickness. Attractive PMMA−silica interfacial interactions increase the T_g, while free surfaces decrease the T_g of PMMA in ultrathin films relative to bulk PMMA. Thus, the significant differences between the T_gs of the 1-D and two-dimensional (2-D) forms of PMMA on silica are the result of a substantial increase in the ratio of free-surface area to interfacial area in the PMMA nanolines relative to ultrathin films.

Miniaturization of devices has led to an array of emerging applications that require polymer nanostructures for diverse disciplines ranging from tissue engineering,[1] molecular electronics,[2] and microfluidic devices[3] to sacrificial templates[4] and photonic materials.[5] The crucial role played by polymer resists for generating sub-100 nm features during the lithographic process in the microelectronics industry is another strong motivating factor for evaluating the properties of polymer nanostructures.[6−8] While the potential benefit of miniaturization is one of the drivers for fabrication of nanostructures, the size-dependent properties observed in several material systems[9−11] necessitates a thorough evaluation of the physical properties of these nanostructures. As in many dimensionally constrained material systems, the physical properties of polymer nanostructures can deviate significantly from those measured in the bulk state. For example, properties of thin polymer films such as the glass-transition temperature (T_g),[12−36] physical aging,[34−39] modulus,[40−45] compliance,[46] and diffusion coefficients[47,48] are seen to deviate from bulk values. In the case of T_g behavior, studies of ultrathin polymer films have included substrate-supported and freely standing films. With some exceptions,[13] when film thickness decreases below a critical value for substrate-supported films, an increase in T_g is generally observed for polymers exhibiting strong attractive interactions with the substrate,[14,17,18,24,30−36] and a decrease in T_g is observed for polymers lacking such attractive interactions with the substrate.[12−17,19,22,25,30,32,33] For freely standing films, T_g generally decreases when thickness decreases below some critical value.[20,21,23]

In contrast to the many studies devoted to the effect of confinement on the properties of thin polymer films,[12−49] there is a notable paucity of research[42−44] focused on the effect of confinement in 1-D polymer nanostructures, and none directly report T_g values. This lack of reports on the T_g of nanostructures is likely due to the fact that many of the experimental methods used to measure T_g in thin and ultrathin films, such as ellipsometry and X-ray reflectivity, are inapplicable to polymer nanostructures. However, such a study is important because the knowledge of how thermophysical properties are altered upon confinement in these nanostructures is vital to the advancement of various nanotechnology applications. The current study is made possible by the first use of an ensemble fluorescence technique, recently developed to characterize distributions of and average T_g values in ultrathin films and nanocomposites,[12−15,33,34,50] to determine T_g values in 1-D nanopatterned systems.

One-dimensional polymer nanostructures can be obtained by various patterning techniques, including imprint lithography,[6,51] dip pen nanolithography,[52,53] photolithography,[54] electrostatic lithography,[55] capillary techniques,[56] and electron

* To whom correspondence should be addressed. E-mail: j-torkelson@northwestern.edu (J.M.T.); v-dravid@northwestern.edu (V.P.D.).
[†] Department of Materials Science and Engineering.
[‡] Department of Chemical and Biological Engineering.

10.1021/nl062894c CCC: $37.00
Published on Web 02/09/2007

beam lithography (EBL).[57] Among these, EBL is attractive because it is a maskless technique that enables one to readily fabricate nanostructures simply by designing the pattern via computer rather than having to prepare different masks, as with other projection lithography techniques. In addition, the poly(methyl methacrylate) (PMMA) system studied in this report is one of the most common electron beam resists with extensive literature (e.g., refs 57−59) on the EBL patterning process that can be readily adopted for our study. The technological relevance of PMMA to the microelectronics industry and the fact that comparisons can be made to studies of the effect of confinement on T_g in PMMA films supported on silica[17,30,31,33−35] are other motivating factors for our choice in studying this system. We employed EBL to fabricate PMMA nanopatterns on silica of various line widths (LW) and thicknesses (h). Here, we report the first study of the effect of 1-D nanopatterned geometry, including nanoline thickness and line width, on T_g in a confined polymer system and compare our results to those of thin films (2-D geometry) of the same thickness. Such an investigation is important because the mechanical robustness of nanopatterned polymers may be affected by reductions in T_g that are associated with the high free-surface (polymer−air interface) area present in nanopatterns.

Poly(methyl methacrylate) labeled with the fluorescent dye 4-tricyanovinyl-[*N*-(2-hydroxyethyl)-*N*-ethyl]aniline (TC1) was synthesized by free radical polymerization of methyl methacrylate (Aldrich) with a trace amount of TC1-labeled methacrylate.[35] The TC1-labeled methacrylate was synthesized by an esterification reaction of TC1 with methacryloyl chloride (Aldrich) in the presence of triethylamine (Aldrich) and dichloromethane (Aldrich) at 0 °C for 2 h. The TC1 was synthesized by a route discussed elsewhere.[60] The resulting TC1-labeled PMMA was washed by multiple dissolution and precipitation steps in toluene and methanol to remove traces of residual unreacted TC1-labeled monomer. The purified TC1-labeled PMMA contained 1.37 mol % (1 in 73 repeat units) TC1-labeled monomer, as determined by UV−vis absorbance spectroscopy (Perkin-Elmer Lambda 35), and had a number-average molecular weight (M_n) of 509 000 g/mol and a polydispersity index (M_w/M_n) of 1.67, as obtained by gel permeation chromatography using universal calibration and polystyrene standards. The bulk T_g of this material was 394 K, as determined by differential scanning calorimetry (Mettler Toledo DSC822e; onset method, second heating cycle at a 10 K/min heating rate) and 395 K, as determined by our fluorescence method.

Phosphorus-doped Si(100) substrates with 140 Å thermal oxide layers were cleaned in a piranha solution (3:1 volume ratio of H_2SO_4 and 30% H_2O_2), thoroughly washed with deionized (DI) water, and rinsed in 2-propanol. Solutions of TC1-labeled PMMA in toluene of various concentrations were spin-coated onto the substrates as a function of spin speed to obtain films of desired thickness.[61] Substrates coated with TC1-labeled PMMA were patterned using a Quanta 600F (FEI Co.) environmental scanning electron microscope integrated with a nanopattern generator lithography system. Samples were exposed to a primary electron beam operating at 10 kV, with a spot size adjusted to give a beam current of 340 pA (±4 pA) and overall doses of 200−400 μC/cm^2. The patterns were developed using a methyl isobutyl ketone:2-propanol (MIBK:IPA) (1:3 volume ratio) solution for 1 min at room temperature. (Separate experiments confirmed that a fine powder of PMMA with M_n = 65 000 g/mol or less dissolved in the developer solution within 1 min. This ensured that the line edges of the final, patterned samples did not contain any low-molecular-weight PMMA with a molecular-weight-dependent T_g.) The patterned samples were imaged using atomic force microscopy (Digital Instruments Nanoscope IIIa) operating in tapping mode with a high-aspect-ratio Si cantilever with a nominal tip radius of 2 nm. After T_g measurement, samples were coated with Au/Pd alloy films of about 10 nm thickness and imaged using the same SEM instrument used for patterning.

The samples for thin film measurements were prepared by spin-coating toluene solutions of TC1-labeled PMMA onto quartz slides; the resulting films were dried in a vacuum oven at ∼5 K above the film T_g for 8 h. Film thicknesses were an average of 10 measurements (standard deviation less than 2%) taken at different locations on the films using a profilmeter (Tencor P10).

Steady-state fluorescence emission spectra were taken as a function of temperature (on cooling) using a Photon Technology International fluorimeter in front-face geometry (with emission at 90° relative to excitation with the sample fixed at a 28° angle relative to excitation) with 3 mm excitation slits (12 nm bandpass) and 3 mm emission slits (6 nm bandpass). The excitation wavelength was 480 nm, and the emission spectra were measured at 540−700 nm. The T_g values were determined from the intersection of linear fits to the temperature dependence of the integrated fluorescence intensity in both the rubbery and glassy states; only data well away from T_g were used for the linear fits, with typical correlation coefficients (R^2) being better than 0.990. The sample temperature was controlled within ±0.1 K using a temperature controller and a flat ribbon heater (Minco Products) mounted on a thin aluminum plate. Additional information on the use of this fluorescence technique to monitor T_g is given in refs 12 and 15.

Optical microscopy images of TC1-labeled PMMA patterns on oxidized Si substrate are shown in Figure 1a. The magnified image in the inset shows the periodicity of the pattern, whereas the low magnification image shows a relatively large field of view of the patterned area. For each sample, these patterns were generated over a 2 mm × 2 mm area by "stitching together" 100 μm × 100 μm areas exposed in a single electron beam exposure run. Using this general scheme, we generated patterned lines with LW ranging from 50 to 1300 nm on films ranging from 15 to 175 nm in thickness. The structural height (thickness) of these patterns is controlled via the initial film thickness achieved by spin-coating.[61]

One of our initial concerns was to evaluate any possible dimensional distortion and discontinuity of patterned lines upon thermal cycling during T_g measurement. In our case, the temperature schedule used to measure T_g involved heating

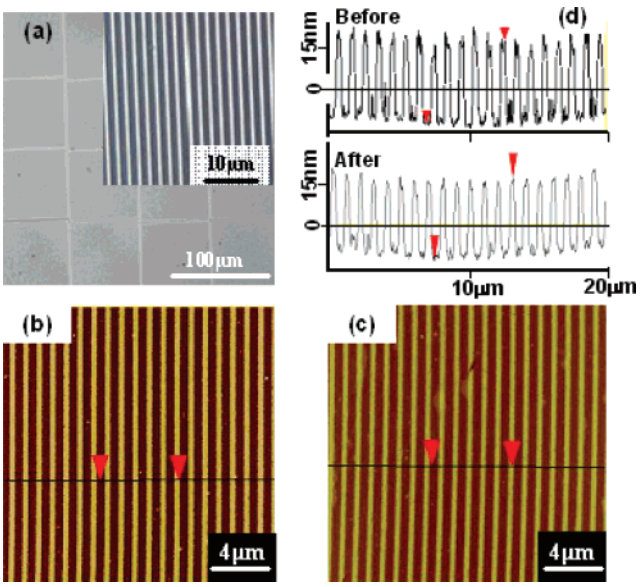

Figure 1. (a) Optical images of TC1-labeled PMMA lines on oxidized Si(100) substrate showing regular order of patterns over large areas and geometry of nanopattern employed in the current study. (b) AFM image of 30-nm-thick pattern with a line width of 260 nm before T_g measurement, and (c) AFM image of the same sample after T_g measurement, demonstrating that lines remain continuous even after thermal cycling through T_g. (d) AFM thickness profile of the same pattern before and after T_g measurement, showing no significant change in line dimensions.

the sample rapidly to a temperature well above T_g ($\sim T_g$ + 25−30 K), holding at temperature for 12 min, and then cooling at a rate of 1.0 K/min to a temperature well below T_g. Figure 1b shows a typical AFM topographic image of a 30-nm-thick nanopattern with $LW = 260$ nm before heating and cooling the sample for T_g measurement, while Figure 1c shows the AFM image of the same sample after T_g measurement. It is clear from these images that the lines remain continuous without any noticeable agglomeration or compaction. Figure 1d shows the AFM profiles of this sample before and after T_g measurement and indicates that, within experimental error, the average pattern height, h, remains unchanged due to thermal cycling associated with the T_g measurement. This implies that the PMMA nanolines are reasonably mechanically robust, with negligible flow of PMMA over the tens of minutes and temperature range employed to measure T_g, including the achievement of temperatures several tens of degrees above T_g. We note that the height profiles in Figure 1d show that the surface roughness within a single line that is less than 3 nm before T_g measurement is reduced further after the T_g measurement, with the surface of the lines becoming smoother on average. This effect may be driven by the surface line tension. Nevertheless, the height and line width of the patterned lines are unchanged by the thermal schedule used in this study. Similar results were obtained with nanolines of various h and LW.

The stability of our PMMA patterns is in stark contrast to the shape evolution or "melting" of PMMA patterns recently reported by Jones et al.[62] This is likely due to several factors. First, the PMMA used by Jones et al. had $M_n = 15\,000$ g/mol. Thus, their sample was below the critical molecular weight for entanglement for PMMA,[63] meaning that a viscous flow response would be expected at temperatures slightly above T_g. (Jones et al.[62] annealed their patterns at 11−20 K above their bulk PMMA T_g.) However, our PMMA sample had $M_n = 509\,000$ g/mol and $M_w = 850\,000$ g/mol. Thus, our PMMA is highly entangled and would be expected to exhibit a rubbery plateau response rather than a viscous flow response at temperatures in excess of T_g in our temperature schedule. Second, the height of our patterns is typically much smaller in our study than the 320 nm initial height associated with the patterns studied by Jones et al.[62] They noted that the rate of pattern relaxation was accelerated at the shortest annealing times where the pattern height was at its maximum. Third, Jones et al.[62] used nanoimprint lithography to make their patterns. The stresses involved in molding their high aspect ratio ($h/LW = 2.5$) patterns are very large, and the shape evolution is driven in part to relieve these stresses. Finally, the presence of a residual layer of PMMA under the patterns made by Jones et al. is also expected to play an important role in the rate of pattern relaxation because, with "large residual layers, the layer acts as an infinite reservoir for the receding patterns."[62]

Ensemble fluorescence is a powerful technique that has been used recently to measure T_g in confined polymer systems.[12−15,33,34,50] With this approach, T_g is identified by the intersection of the liquid-state and glassy-state temperature dependences of the fluorescence of a probe that is doped into or covalently attached to the polymer at trace levels. The measurements are made upon cooling from temperatures above T_g, which means that the T_g measurement is made after erasing thermal history and relaxing some of the stresses induced during sample preparation.[32,64] Figure 2a shows the fluorescence spectra of 18-nm-thick TC1-labeled PMMA nanolines with LW of 50 nm at two different temperatures. The probability of excited-state chromophores returning to the ground state via nonradiative decay increases with temperature and nanoscale mobility in the system, which results in a significant reduction in fluorescence intensity with increasing temperature. The TC1 chromophore is a "rotor" probe[60] that de-excites nonradiatively by rotational motion, as depicted in the inset in Figure 2a; the inset shows the structure of the TC1-labeled monomer used to make TC1-labeled PMMA.

Figure 2b shows the normalized integrated emission intensity as a function of temperature of the TC1-labeled PMMA in an 18-nm-thick film and an 18-nm-thick nanopattern with $LW = 50$ nm. Lines are fit to data points deep in the rubbery and glassy states. The T_g is identified by the intersection of the linear fits to the glassy-state and rubbery-state data.[12,15] The 18-nm-thick TC1-labeled PMMA film exhibits a T_g of 405 K, which is 10 K higher than the T_g of bulk TC1-labeled PMMA. (The bulk PMMA T_g of 395 K is depicted by the vertical dotted line in Figure 2b.) In contrast, a nanostructured, patterned geometry with the same 18 nm thickness and $LW = 50$ nm exhibits a T_g of 390 K, which is 5 K lower than the T_g of bulk TC1-labeled PMMA.

The 10 K increase in T_g relative to bulk of the 18-nm-thick TC1-labeled PMMA film is in excellent agreement with

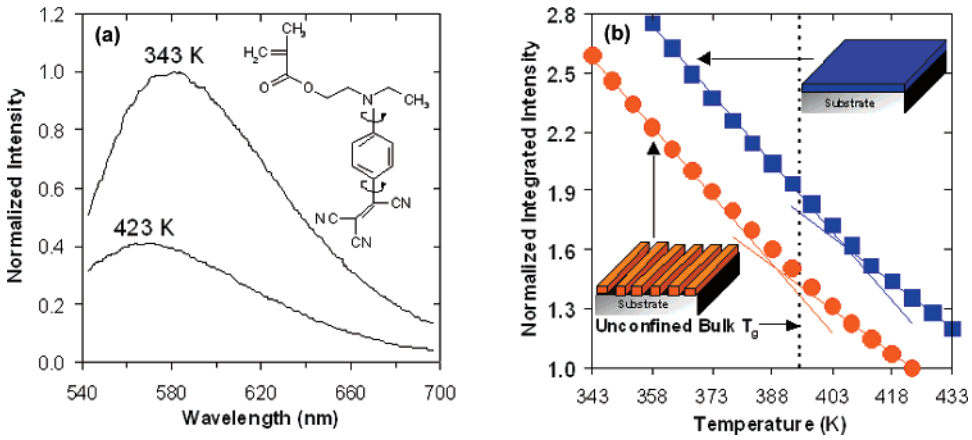

Figure 2. (a) Fluorescence emission spectra of an 18-nm-thick nanopattern of TC1-labeled PMMA with a line width of 50 nm measured at 423 and 343 K. The intensities have been normalized by the peak intensity at 343 K. The inset shows the structure of TC1-labeled monomer used in making TC1-labeled PMMA. (b) Temperature dependence of integrated fluorescence intensity of TC1-labeled PMMA: 18-nm-thick film (squares) and 18 nm thick nanolines with $LW = 50$ nm (circles). (The integrated intensity has been normalized to the peak intensity at 433 and 423 K, respectively, and shifted vertically for clarity.) The intersection of vertical dotted line with x-axis represents the T_g of PMMA in bulk form. Inset show schematics of both sample geometries.

other results obtained regarding the effect of decreasing thickness on T_g in PMMA films supported on silica substrates.[17,31] This effect is understood to arise from attractive interfacial interactions resulting from hydrogen bond formation between hydroxyl groups naturally present on the silica surface and the ester side groups in PMMA.[17,30,31,35,36] The hydrogen bonds reduce cooperative segmental mobility and thereby lead to an increase in T_g in ultrathin films.

In contrast, the result showing the 5 K reduction in T_g relative to bulk in the 18-nm-thick PMMA nanolines with LW of 50 nm is the first of its kind. This effect may be understood to arise from the fact that the 18-nm-thick nanopatterned system has a much higher free-surface (polymer−air interface) area than the 18-nm-thick ultrathin film. In the case of the nanopatterned PMMA system, the ability of the free surface to yield a reduction in T_g[23] is in competition with ability of the attractive interactions at the polymer−substrate interface to yield an increase in T_g.[17,30,31,35,36] Because of the much greater free-surface area relative to the polymer−substrate interfacial area, on balance, the free-surface effects are dominant and lead to a reduced T_g in the nanopatterned geometry. This result illustrates the importance of confining geometry in defining the nature of T_g in confined systems.

To further validate the competing effects of free-surface area and PMMA−silica interfacial area on T_g, we measured the T_g values of PMMA nanopatterns with various geometries. Figure 3 summarizes the effects of film thickness and pattern geometry (LW) on the T_g of TC1-labeled PMMA films and nanopatterns. Consistent with previously published data on PMMA ultrathin films,[17,30,31,35,36] at thicknesses less than 80−90 nm, we find that the T_gs of the PMMA films increase with decreasing thickness, with an 18-nm-thick film exhibiting a 10 K increase relative to the bulk T_g. In the case of our patterned lines made by EBL, when h is 175 nm and LW values are 400, 760, or 1000 nm, the T_gs are nearly identical to bulk T_g. (Values of LW are shown in parentheses in Figure 3.) In these cases, the added free-surface area in the patterned lines is insufficient to perturb the value of T_g

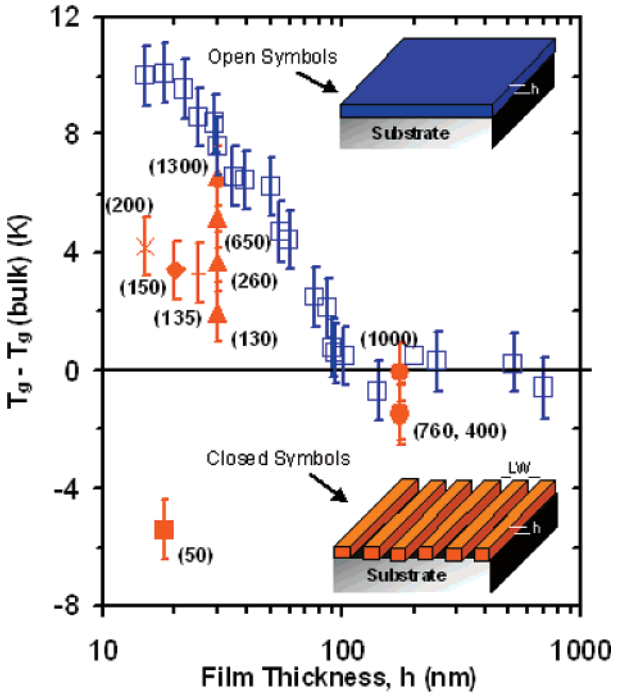

Figure 3. $T_g - T_g$(bulk) as a function of film thickness for TC1-labeled PMMA films (open squares) and nanolines with thickness of 175 nm (●), 30 nm (▲), 25 nm (+), 20 nm (♦), 18 nm (□), and 15 nm (×), respectively. The numbers in parentheses specify the line widths (LW). The error bars correspond to the error (±1 K) in estimating T_g values by the intersection of linear temperature dependences of integrated intensity in the rubbery and glassy states. The insets show schematics of sample geometries employed for T_g characterization.

from that of the 175-nm-thick film from which they were made. In contrast, significant perturbations to T_g are observed in 30-nm-thick nanolines with $LW = 130$ nm, with a 5 K difference in T_g being apparent in systems with LW values of 130 and 1300 nm. The reduction in T_g with decreasing LW is because of the increasing effects of the free surface that compete with the effects of attractive polymer−substrate interactions.

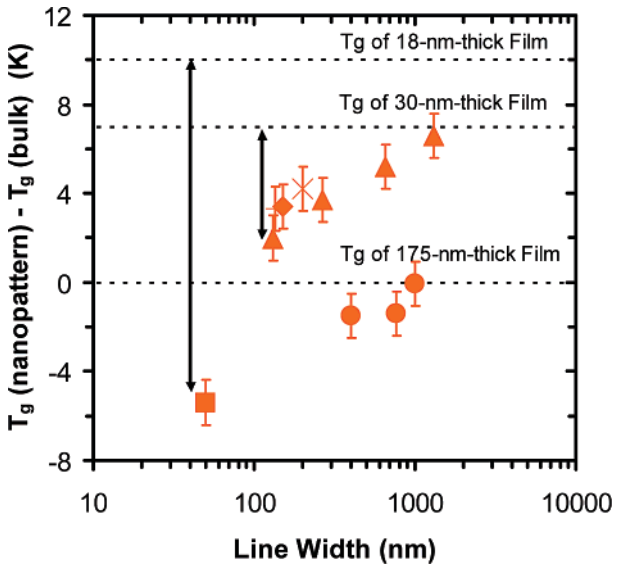

Figure 4. T_g(nanopattern) − T_g(bulk) as a function of line width for nanolines of various thickness: 175 nm (●), 30 nm (▲), 25 nm (+), 20 nm (♦), 18 nm (■), and 15 nm (×). The horizontal dotted lines show the values of T_g for the corresponding thin films of particular thicknesses relative to that of bulk PMMA. The error bars correspond to the error (±1 K) in estimating T_g.

Striking effects are observed in the 15-nm-thick and 18-nm-thick patterned lines. In a 15-nm-thick pattern with LW = 200 nm, T_g is increased by ∼4 K relative to bulk T_g and is reduced by ∼6 K relative to the T_g of a 15-nm-thick PMMA film. These results are indicative of the competition between free-surface and polymer−substrate effects, with the polymer−substrate effect dominating the free-surface effects in the patterned system. On the other hand, in an 18-nm-thick nanopattern with LW = 50 nm, T_g is reduced by ∼5 K relative to bulk T_g (T_g(bulk)) and by ∼15 K relative to the T_g of an 18-nm-thick PMMA film. In this case, the effects of the free surface present on three sides of the nanolines dominate over the effect of attractive polymer−substrate interactions present on the fourth side of the nanolines.

We note that these results can be rationalized based on measurements by Roth and Dutcher[23] of the thickness dependence of T_g of freely standing PMMA films, with two free surfaces and no substrate. Using a nearly monodisperse PMMA sample with M_w = 790 000 g/mol, close to the M_w value of 850 000 g/mol for our TC1-labeled PMMA, they observed a reduction in T_g of ∼15 K relative to that of bulk PMMA in a 50-nm-thick freely standing PMMA film. Our 18-nm-thick nanopattern with LW = 50 nm exhibits T_g = T_g(bulk) − 5 K, i.e., 10 K above that of their 50-nm-thick freely standing PMMA film. The increase in our nanopattern T_g relative to that of the freely standing films arises from the attractive substrate interactions that are present in the nanopattern and absent in the freely standing film.

To represent more simply the effect of the ratio of free-surface area to PMMA−silica interfacial area in modifying the T_g of the nanopatterns relative to the thin or ultrathin films from which they were made, the data in Figure 3 are replotted in Figure 4. The latter figure emphasizes the variations in T_g of the 1-D-patterned nanostructures with various LWs compared to the thin films having the same thickness.

These results demonstrate that the knowledge of how confinement modifies T_g in supported polymer films (2-D case) cannot be simply extended without modification to predict the T_g behavior of polymer 1-D nanopatterns supported on a substrate. This is because the properties of the patterned polymer 1-D nanostructures are influenced by the combined effects of the free surfaces and the attractive substrate interactions. This means that the detailed geometry must be considered in any experimental studies or simulations of the thermal properties of such nanostructures. Furthermore, given that the strength of the attractive polymer−substrate interactions can be tuned by modification of the substrate surface[30] and polymer or copolymer composition,[31,33] the magnitude of the interaction must be carefully accounted for in any simulation of nanostructure physical or mechanical properties. We also note that our experimental T_g results are qualitatively consistent with a recent simulation study[41] of apparent modulus of polymer nanostructures, which reported that the elastic constants show a significant reduction from bulk behavior with decreasing line width, and that the surface-to-volume ratio is a key parameter in defining the nanostructure properties.

In summary, this is the first report of the determination of T_g as a function of confinement in 1-D polymer nanostructures. With PMMA nanolines supported on silica, the important roles of the ratio of free-surface area to polymer−substrate interface area and the attractive polymer−substrate interactions in defining the nanostructure T_g are demonstrated. Attractive polymer−substrate interactions result in a substantial increase of T_g with decreasing thickness in ultrathin PMMA films. However, when such attractive polymer−substrate interactions are present in nanopatterned polymers, an increase in the ratio of free-surface area to the polymer−substrate interfacial area can substantially reduce the T_g of 1-D nanostructures supported on a substrate, even to temperatures below the T_g of the bulk polymer.

Acknowledgment. This work is supported by the NSF-MRSEC program at Northwestern University (grants DMR-0076097 and DMR-0520513) and Northwestern University. A part of this work was performed in the EPIC, NIFTI, Keck-II facility of the NU*ANCE* Center at Northwestern University. The NU*ANCE* Center is supported by NSF-NSEC, NSF-MRSEC, Keck Foundation, the State of Illinois, and Northwestern University. Any opinions, findings and conclusions or recommendations expressed in this material are those of the authors and do not necessarily reflect those of the National Science Foundation.

References

(1) Griffith, L. G.; Naughton, G. *Science* **2002**, *295*, 1009.
(2) Huang, Y.; Duan, X. F.; Wei, Q. Q.; Lieber, C. M. *Science* **2001**, *291*, 630.
(3) Therriault, D.; White, S. R.; Lewis, J. A. *Nat. Mater.* **2003**, *2*, 265.
(4) Xia, Y. N.; Rogers, J. A.; Paul, K. E.; Whitesides, G. M. *Chem. Rev.* **1999**, *99*, 1823.
(5) Lin, S. Y.; Fleming, J. G.; Hetherington, D. L.; Smith, B. K.; Biswas, R.; Ho, K. M.; Sigalas, M. M.; Zubrzycki, W.; Kurtz, S. R.; Bur, J. *Nature* **1998**, *394*, 251.

(6) Resnick, D. J.; Dauksher, W. J.; Mancini, D.; Nordquist, K. J.; Bailey, T. C.; Johnson, S.; Stacey, N.; Ekerdt, J. G.; Willson, C. G.; Sreenivasan, S. V.; Schumaker, N. *J. Vac. Sci. Technol., B* **2003**, *21*, 2624.
(7) Bratton, D.; Yang, D.; Dai, J. Y.; Ober, C. K. *Polym. Adv. Technol.* **2006**, *17*, 94.
(8) Marceau, S.; Tortai, J.-H.; Tillier, J.; Vourdas, N.; Gogolides, E.; Raptis, I.; Beltsios, K.; van Werden, K. *Microelectron. Eng.* **2006**, *83*, 1073.
(9) Zhu, J.; Somorjai, G. A. *Nano Lett.* **2001**, *1*, 8.
(10) Alivisatos, A. P. *Science* **1996**, *271*, 933.
(11) Li, L.; Hu, J.; Yang, W.; Alivisatos, A. P. *Nano Lett.* **2001**, *1*, 349.
(12) Ellison, C. J.; Mundra, M. K.; Torkelson, J. M. *Macromolecules* **2005**, *38*, 1767.
(13) Ellison, C. J.; Ruszkowski, R. L.; Fredin, N. J.; Torkelson, J. M. *Phys. Rev. Lett.* **2004**, *92*, 095702.
(14) Ellison, C. J.; Torkelson, J. M. *J. Polym. Sci., Part B: Polym. Phys.* **2002**, *40*, 2745.
(15) Ellison, C. J.; Torkelson, J. M. *Nat. Mater.* **2003**, *2*, 695.
(16) Keddie, J. L.; Jones, R. A. L.; Cory, R. A. *Europhys. Lett.* **1994**, *27*, 59.
(17) Keddie, J. L.; Jones, R. A. L.; Cory, R. A. *Faraday Discuss.* **1994**, *98*, 219.
(18) van Zanten, J. H.; Wallace, W. E.; Wu, W. L. *Phys. Rev. E* **1996**, *53*, R2053.
(19) Kawana, S.; Jones, R. A. L. *Phys. Rev. E* **2001**, *63*, 021501.
(20) Dalnoki-Veress, K.; Forrest, J. A.; de Gennes, P. G.; Dutcher, J. R. *J. Phys. IV* **2000**, *10*, 221.
(21) Forrest, J. A.; Dalnoki-Veress, K.; Stevens, J. R.; Dutcher, J. R. *Phys. Rev. Lett.* **1996**, *77*, 2002.
(22) Sharp, J. S.; Forrest, J. A. *Phys. Rev. Lett.* **2003**, *91*, 235701.
(23) Roth, C. B.; Dutcher, J. R. *Eur. Phys. J. E* **2003**, *12*, S103.
(24) Grohens, Y.; Hamon, L.; Reiter, G.; Soldera, A.; Holl, Y. *Eur. Phys. J. E* **2002**, *8*, 217.
(25) Pratt, F. L.; Lancaster, T.; Brooks, M. L.; Blundell, S. J.; Proksch a, T.; Morenzoni, E.; Suter, A.; Luetkens, H.; Khasanov, R.; Scheuermann, R.; Zimmermann, U.; Shinotsuka, K.; Assender, H. E. *Phys. Rev. B* **2005**, *72*, 121401.
(26) Serghei, A.; Mikhailova, Y.; Huth, H.; Schick, C.; Eichhorn, K. J.; Voit, B.; Kremer, F. *Eur. Phys. J. E* **2005**, *17*, 199.
(27) Baschnagel, J.; Varnik, F. *J. Phys.: Condens. Matter* **2005**, *17*, R851.
(28) Jain, T. S.; de Pablo, J. J. *Phys. Rev. Lett.* **2004**, *92*, 155505.
(29) Campoy-Quiles, M.; Sims, M.; Etchegoin, P. G.; Bradley, D. D. C. *Macromolecules* **2006**, *39*, 7673.
(30) Fryer, D. S.; Peters, R. D.; Kim, E. J.; Tomaszewski, J. E.; de Pablo, J. J.; Nealey, P. F.; White, C. C.; Wu, W. L. *Macromolecules* **2001**, *34*, 5627.
(31) Park, C. H.; Kim, J. H.; Ree, M.; Sohn, B. H.; Jung, J. C.; Zin, W. C. *Polymer* **2004**, *45*, 4507.
(32) Mundra, M. K.; Ellison, C. J.; Behling, R. E.; Torkelson, J. M. *Polymer* **2006**, *47*, 7747.
(33) Mundra, M. K.; Ellison, C. J.; Rittigstein, P.; Torkelson, J. M. *Eur. Phys. J. Spec. Top.* **2007**, *141*, 143.
(34) Ellison, C. J.; Kim, S. D.; Hall, D. B.; Torkelson, J. M. *Eur. Phys. J. E* **2002**, *8*, 155.
(35) Priestley, R. D.; Ellison, C. J.; Broadbelt, L. J.; Torkelson, J. M. *Science* **2005**, *309*, 456.
(36) Priestley, R. D.; Broadbelt, L. J.; Torkelson, J. M. *Macromolecules* **2005**, *38*, 654.
(37) Kawana, S.; Jones, R. A. L. *Eur. Phys. J. E* **2003**, *10*, 223.
(38) Huang, Y.; Paul, D. R. *Macromolecules* **2006**, *39*, 1554.
(39) Fukao, K.; Sakamoto, A. *Phys. Rev. E* **2005**, *71*, 041803.
(40) Yoshimoto, K.; Jain, T. S.; Nealey, P. F.; de Pablo, J. J. *J. Chem. Phys.* **2005**, *122*, 144712.
(41) Van Workum, K.; de Pablo, J. J. *Nano Lett.* **2003**, *3*, 1405.
(42) Stafford, C. M.; Vogt, B. D.; Harrison, C.; Julthongpiput, D.; Huang, R. *Macromolecules* **2006**, *39*, 5095.
(43) Hartschuh, R. D.; Kisliuk, A.; Novikov, V.; Sokolov, A. P.; Heyliger, P. R.; Flannery, C. M.; Johnson, W. L.; Soles, C. L.; Wu, W. L. *Appl. Phys. Lett.* **2005**, *87*, 173121.
(44) Hartschuh, R.; Ding, Y.; Roh, J. H.; Kisliuk, A.; Sokolov, A. P.; Soles, C. L.; Jones, R. L.; Hu, T. J.; Wu, W. L.; Mahorowala, A. P. *J. Polym. Sci., Part B: Polym. Phys.* **2004**, *42*, 1106.
(45) Stafford, C. M.; Harrison, C.; Beers, K. L.; Karim, A.; Amis, E. J.; Vanlandingham, M. R.; Kim, H. C.; Volksen, W.; Miller, R. D.; Simonyi, E. E. *Nat. Mater.* **2004**, *3*, 545.
(46) O'Connell, P. A.; McKenna, G. B. *Eur. Phys. J. E* **2006**, *20*, 143.
(47) Frank, B.; Gast, A. P.; Russell, T. P.; Brown, H. R.; Hawker, C. *Macromolecules* **1996**, *29*, 6531.
(48) Hall, D. B.; Torkelson, J. M. *Macromolecules* **1998**, *31*, 8817.
(49) O'Connell, P. A.; McKenna, G. B. *Science* **2005**, *307*, 1760.
(50) Rittigstein, P.; Torkelson, J. M. *J. Polym. Sci., Part B: Polym. Phys.* **2006**, *44*, 2935.
(51) Chou, S. Y.; Krauss, P. R.; Renstrom, P. J. *Science* **1996**, *272*, 85.
(52) Piner, R. D.; Zhu, J.; Xu, F.; Hong, S. H.; Mirkin, C. A. *Science* **1999**, *283*, 661.
(53) Noy, A.; Miller, A. E.; Klare, J. E.; Weeks, B. L.; Woods, B. W.; DeYoreo, J. J. *Nano Lett.* **2002**, *2*, 109.
(54) Xu, J.; Xia, H. P.; Zhang, Y. P.; Zhang, J. L.; Wang, J. H. *J. Inorg. Mater.* **2005**, *20*, 193.
(55) Lyuksyutov, S. F.; Vaia, R. A.; Paramonov, P. B.; Juhl, S.; Waterhouse, L.; Ralich, R. M.; Sigalov, G.; Sancaktar, E. *Nat. Mater.* **2003**, *2*, 468.
(56) Donthu, S. K.; Pan, Z.; Shekhawat, G. S.; Dravid, V. P.; Balakrisnan, B.; Tripathy, S. *J. Appl. Phys.* **2005**, *98*, 024304.
(57) Donthu, S.; Pan, Z. X.; Myers, B.; Shekhawat, G.; Wu, N. G.; Dravid, V. *Nano Lett.* **2005**, *5*, 1710.
(58) Chen, W.; Ahmed, H. *Appl. Phys. Lett.* **1993**, *62*, 1993.
(59) Dobisz, E. A.; Brandow, S. L.; Bass, R.; Mitterender, J. *J. Vac. Sci. Technol.* **2000**, *18*, 107.
(60) Hooker, J. C.; Torkelson, J. M. *Macromolecules* **1995**, *28*, 7683.
(61) Hall, D. B.; Underhill, P.; Torkelson, J. M. *Polym. Eng. Sci.* **1998**, *38*, 2039.
(62) Jones, R. L.; Hu, T.; Soles, C. L.; Lin, E. K.; Reano, R. M.; Pang, S. W.; Casa, D. M. *Nano Lett.* **2006**, *6*, 1723.
(63) Fuchs, K.; Friedrich, C.; Weese, J. *Macromolecules* **1996**, *29*, 5893.
(64) With many of the nanopatterns, we made a second measurement of T_g immediately after the first measurement. If there were any residual organic-based developer left in the nanopatterns which could affect T_g, some or all of it would be removed during the first T_g measurement and reheating to perform the second T_g measurement. However, the measured T_gs were identical in the first and second measurements, indicating that, within experimental uncertainty, there was no influence of exposure of the PMMA to the developer on the thermal response of the final, nanostructured films.

NL062894C